ELSEVIER

Remote Sensing of Environment 83 (2002) 431–441

Remote Sensing of Environment

www.elsevier.com/locate/rse

Multiscale analysis and validation of the MODIS LAI product II. Sampling strategy

Yuhong Tian[a,b,*], Curtis E. Woodcock[a], Yujie Wang[a], Jeff L. Privette[c], Nikolay V. Shabanov[a], Liming Zhou[b], Yu Zhang[a], Wolfgang Buermann[a], Jiarui Dong[a], Brita Veikkanen[d], Tuomas Häme[d], Kaj Andersson[d], Mutlu Ozdogan[a], Yuri Knyazikhin[a], Ranga B. Myneni[a]

[a] *Department of Geography, Boston University, Boston, MA 02215, USA*
[b] *School of Earth and Atmospheric Sciences, Georgia Institute of Technology, Atlanta, GA 30332, USA*
[c] *Code 923, NASA Goddard Space Flight Center, Greenbelt, MD 20771, USA*
[d] *VTT AUTOMATION, Remote Sensing, 02044 VTT, Finland*

Received in revised form 5 April 2002; accepted 7 April 2002

Abstract

The development of appropriate ground-based validation techniques is critical to assessing uncertainties associated with satellite data-based products. In this paper, the second of a two-part series, we present a method for validation of the Moderate Resolution Imaging Spectroradiometer Leaf Area Index (MODIS LAI) product with emphasis on the sampling strategy for field data collection. Using a hierarchical scene model, we divided 30-m resolution LAI and NDVI images from Maun (Botswana), Harvard Forest (USA) and Ruokulahti Forest (Finland) into individual scale images of classes, region and pixel. Isolating the effects associated with different landscape scales through decomposition of semivariograms not only shows the relative contribution of different characteristic scales to the overall variation, but also displays the spatial structure of the different scales within a scene. We find that (1) patterns of variance at the class, region and pixel scale at these sites are different with respect to the dominance in order of the three levels of landscape organization within a scene; (2) the spatial structure of LAI shows similarity across the three sites, that is, ranges of semivariograms from scale of pixel, region and class are less than 1000 m. Knowledge gained from these analyses aids in formulation of sampling strategies for validation of biophysical products derived from moderate resolution sensors such as MODIS. For a homogeneous (within class) site, where the scales of class and region account for most of the spatial variation, a sampling strategy should focus more on using accurate land cover maps and selection of regions. However, for a heterogeneous (within class) site, accurate point measurements and GPS readings are needed.

1. Introduction

The Terra satellite was launched in December 1999 and first Earth views from the Moderate Resolution Imaging Spectroradiometer (MODIS) were taken in late February 2000. As MODIS Leaf Area Index (LAI) data become publicly available through the EROS Data Center Data Active Archive Center (EDC DAAC), product quality must be ensured through validation.

"Validation" is the process of assessing by independent means the accuracy (uncertainty) of data products (Justice et al., 2000; Privette et al., 2000). However, uncertainty assessment of these coarse spatial resolution products is not straightforward, and presents a challenge to the remote sensing community because ground-based measurements cannot be easily compared to coarse resolution satellite sensor data (Weiss et al., 2001). Development of appropriate ground-based validation techniques and sampling strategy is therefore critical to assessing the uncertainties associated with such data products. The main challenge in land satellite data validation is to attain adequate ground sampling of observed biophysical variables, which exhibit spatial and temporal variance, at the spatial scale of a satellite sensor (Lucht et al., 2000). In addition, large-scale validation should rely on methods that avoid time-consuming procedures while preserving accuracy.

* Corresponding author. School of Earth and Atmospheric Sciences, Georgia Institute of Technology, 221 Bobby Dodd Way, Atlanta, GA 30332, USA. Tel.: +1-404-385-2383; fax: +1-404-385-1510.
E-mail address: ytian@eas.gatech.edu (Y. Tian).

0034-4257/02/$ - see front matter © 2002 Elsevier Science Inc. All rights reserved.
PII: S0034-4257(02)00058-5

In this two-part series, we attempt to assess the uncertainty of the MODIS LAI product via comparisons with ground and high-resolution satellite data, and provide guidance for field data collection and sampling strategies. In the first paper of this two-part series (Tian et al., 2002) we propose a region- or patch-based comparison method and address the issue of spatially scaling ground-based point measurements to the spatial scale of satellite observations. We also provide comparisons of validated 30 m ETM+ LAI retrievals to those derived from the 250-m, 500-m and 1-km resolutions of simulated MODIS data. Based on our experience from analyses of SAFARI 2000 data, it was concluded that improvements are needed regarding field data sampling. The objective of this paper is to design a statistically valid and logistically feasible field sampling strategy.

Woodcock, Strahler, and Jupp (1988a,b) observed that image semivariograms are diagnostic of scene structure. Curran (1988) suggested that semivariograms in remote sensing could help selection of spatial resolution and design of sampling schemes. In this paper, hierarchical decomposition of LAI images, coupled with analysis of the component semivariograms, reveals information about LAI variation over different scales, which in turn aids in the formulation of sampling strategies for validation. In addition, we demonstrate the dominant factors that influence the spatial distribution of LAI across the landscape, and provide guidance for field data collection and sampling strategies.

2. Hierarchical analysis of multiscale variation in images

2.1. Semivariogram

Semivariogram, which measures semivariance as a function of distance, is a useful measure of the spatial structure of images (Curran, 1988; Woodcock, Collins, & Jupp, 1997). For a stationary and isotropic spatial process, the semivariance $\gamma(h)$ in Z values between all the pairs of points $Z(x)$ and $Z(x+h)$ separated by distance h (referred to as "lag") can be estimated as,

$$\gamma(h) = \frac{1}{2N(h)} \sum_{N(h)} [Z(x+h) - Z(x)]^2. \quad (1)$$

Here N is the number of pairs of sample points $(x, x+h)$ separated by distance h. A plot of semivariance, $\gamma(h)$, as a function of distance h, is semivariogram. There are two important features noteworthy in the semivariogram. First, with distance h increasing, semivariance tends to rise from zero to the level of the global variance of the image, and then levels off. This constant value (global variance) is referred to as the "sill". Second, the value of h at which the semivariogram reaches the sill is called the range of influence, and is related to the size of objects in the image. Beyond this range, there is no relation between two pixels. Within this range, Z values are more similar when the pairs of sample points are closer together. The range and sill together can help in describing the spatial variation and structure of an image. Eq. (1) can be used to calculate a semivariogram from any image, for example, LAI and NDVI images in this study.

2.2. Hierarchical decomposition of scene semivariograms

A key to scaling in remote sensing is to understand the magnitude of the effects resulting from processes acting at different scales in the landscape (Woodcock et al., 1997). Nested-hierarchical models can be used to partition variance in an image at different levels. In a hierarchical model of landscapes, each level in the hierarchy corresponds to a different scale. In a forested landscape, for example, the most fundamental element might be individual trees. The next level might be patches or stands of trees. All patches of the same kind would combine to form forest classes, which would be a third level in the hierarchy. These different forest types might then combine to form a general class of forest, which exists with other classes at this level, such as grassland, water, savanna, etc. Therefore, each successive level in the hierarchy is more general and is formed by combining elements from the levels below (Woodcock et al., 1997).

A nested-hierarchical model of spatial data is provided by Moellering and Tobler (1972) and is elaborated by Woodcock et al. (1997) and Collins and Woodcock (2000). Under this theory, the hierarchical model describes the image as being composed of a number of land cover classes, D_i, which are defined as disjoint subsets of the entire image D. Each class D_i is in turn composed of a number of regions (D_{ij}). Note that "region" as defined here has the same meaning as "patch," mentioned in the previous paper (Tian et al., 2002). Regions are composed of pixels, denoted D_{ijk} (Woodcock et al., 1997; Collins & Woodcock, 2000). The mean of the entire image, for example LAI or NDVI image, is $\mu(D)$. The mean of a class at the first level of the hierarchy is $\mu(D_i)$, and the mean of a region at the second level of the hierarchy is $\mu(D_{ij})$. Under this assumption, the observed pixel values may be defined as

$$Z(m,n) = x_{ijk} = D_{ijk}, \quad (2)$$

where variables m and n represent the pixel's position (row m and column n) in the image.

A set of four new images, which are derivatives of the original image, can therefore be created and these images contain only the effects associated with an individual scale, or level in the hierarchy. They are image scale (I), class scale (C), region scale (R), and pixel scale (P) images, respectively. Pixel values for these new images,

$Z\alpha$ ($\alpha = I, C, R, P$), can be calculated as (Woodcock et al., 1997).

$$Z_I(m,n) = I = \mu(D), \tag{3}$$

$$Z_C(m,n) = C_i = \mu(D_i) - \mu(D), \tag{4}$$

$$Z_R(m,n) = R_{ij} = \mu(D_{ij}) - \mu(D_i), \tag{5}$$

$$Z_P(m,n) = P_{ijk} = x_{ijk} - \mu(D_{ij}). \tag{6}$$

Here I is the image effect, C_i is the effect associated with class i, R_{ij} is the effect associated with region j of class i, and P_{ijk} is the residual or pixel effect associated with pixel k of region j of class i. Fig. 1 is an example of a LAI image, which consists of three classes, D_1, D_2 and D_3. Each class consists of several regions. For D_1, there are three regions; for D_2, two regions. Each region contains many pixels. Fig. 1(a) shows the class effect image (Eq. (4)), in which all pixels belonging to the same class have the same value of LAI. Fig. 1(b) is the region effect image (Eq. (5)), in which all pixels belonging to the same region have the same value of LAI. Pixels located in different regions have different LAI values, even though they might be the same land cover class. Following this theory, any original image can be decomposed into four individual images. They correspond to image effect, class effect, region effect, and pixel effect, respectively. Each image contains only the effect associated with the individual scale. Adding the above four equations indicates that an observed pixel value is equal to the sum of the effects of all levels of the hierarchy:

$$Z(m,n) = x_{ijk} = I + C_i + R_{ij} + P_{ijk} = \sum_{\alpha=I,C,R,P} Z_\alpha(m,n). \tag{7}$$

According to Woodcock et al. (1997), this ordering of levels by area size can be taken as a surrogate for scale or resolution. Data at different levels of the hierarchy thus correspond to different geographical or characteristic scales. Squaring both sides of Eq. (7) and taking the mathematical expectation lead to the basic result of the hierarchical Analysis of Variance (ANOVA) model,

$$\sigma^2 = \sigma_C^2 + \sigma_R^2 + \sigma_P^2. \tag{8}$$

Here, σ^2 is the overall data variance, and σ_α^2 ($\alpha = C, R, P$) is the variance of class, region and pixel effects, respectively. The total variance of the data is the sum of the variances of the individual effects. Eq. (8) indicates how the total variance is partitioned into components corresponding to each of these scales. To apply this model, data must first be organized hierarchically.

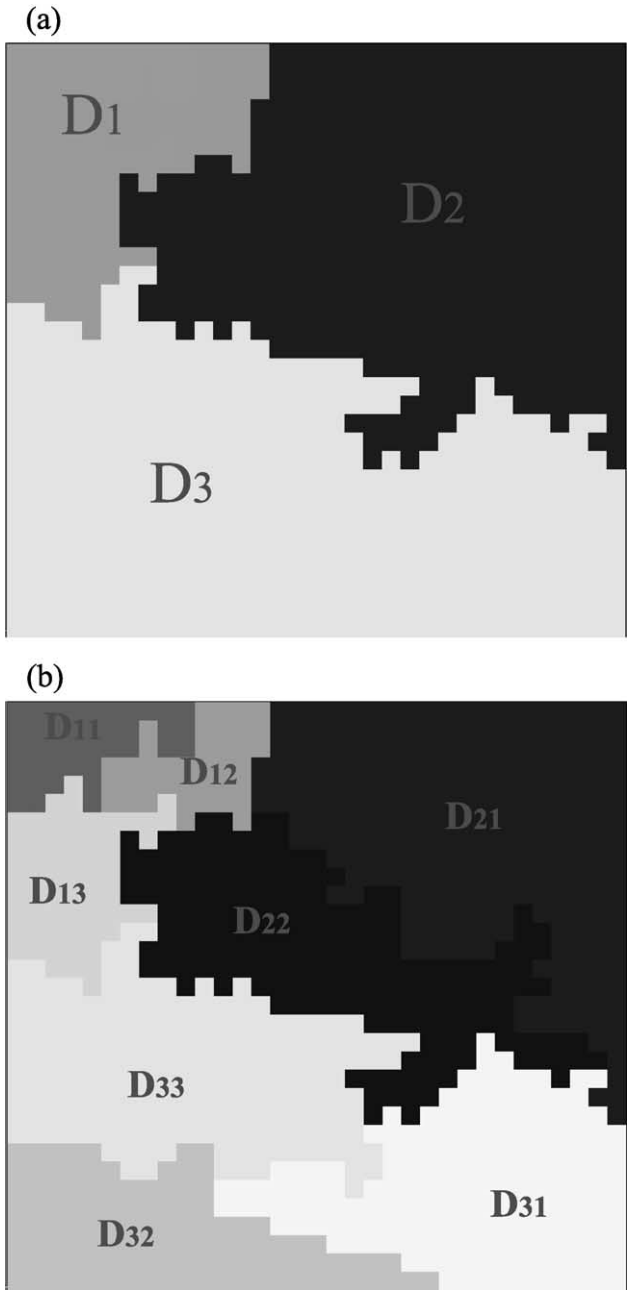

Fig. 1. An example of a LAI image, consisting of three classes, D_1, D_2, and D_3. Classes D_1 and D_3 have three regions, while class D_2 has two regions. Each region contains many pixels. (a) The class effect image, in which all pixels belonging to the same class have the same value of LAI. (b) The region effect image, in which all pixels belonging to the same region have the same value of LAI.

Eq. (1) then can be used to calculate the semivariance for these decomposed images to create separate semivariograms for each γ_I, γ_C, γ_R and γ_P, i.e.,

$$\gamma_\alpha(h) = \frac{1}{2N_\alpha(h)} \sum_{N_\alpha(h)} [Z_\alpha(m+h_m, n+h_n) - Z_\alpha(m,n)]^2, \tag{9}$$

where $\alpha = I, C, R, P, h_m$ and h_n are the distance in pixels in the row and column direction between the two compared pixels, and $h = \text{resolution}\sqrt{h_m^2 + h_n^2}$.

According to Collins and Woodcock (2000), the semivariance for the original image, γ, can be decomposed as

$$\gamma(h) = \gamma_C(h) + \gamma_R(h) + \gamma_P(h) + 2\gamma_{CR}(h) + 2\gamma_{CP}(h) + 2\gamma_{RP}(h), \quad (10)$$

where the subscripts are the same as in Eq. (8). Symbols with single subscript are semivariograms, and symbols with two subscripts are cross-semivariograms. The cross-semivariograms between hierarchical effects are usually small (Collins & Woodcock, 2000) and are ignored here. As is well known, validation efforts can be undertaken at a broad range of observation scales. Efforts will likely be successful when the observation scales are chosen to capture the variation at the characteristic scale of interest.

3. Satellite and field data

In this study, we use three 30-m LAI fields retrieved from ETM+ data. The corresponding ETM+ data are related to three field sites as described below. The three sites are savanna in Maun, Botswana (Fig. 2); broadleaf forests in the Harvard Forest (Fig. 3), USA; and needleleaf forests in the Ruokolahti Forest (Fig. 4), Finland. The Maun site is located at 19.9229°S, 23.5943°E. The main vegetation types are savanna and shrubs (Tian et al., 2002). The Harvard Forest research site is located at 42.5382°N, 72.1714°W. It includes mixed hardwood and conifer forests, ponds, extensive spruce and maple swamps, with pine and hemlock, and conifer plantations. The Ruokolahti Forest site is a typical northern needleleaf forest (61.5263°N, 28.7103°E), mixed with large and small lakes.

Following the procedures described in Tian et al. (2002) that utilized 10 × 10 km ETM+ data to validate the MODIS LAI (Knyazikhin, Martonchik & Myeni et al., 1998; Knyazikhin et al., 1998; Knyazikhin et al., 1999) in Maun, a 15 × 13 km (10 km by 10 km) ETM+ image, acquired on August 31, 1999 (June 10, 2000), was used to validate the algorithm at 30-m resolution in the Harvard (Ruokolahti) Forest site. First, the raw data of Band 3 (red) and Band 4 (NIR) from both sites were atmospherically corrected using the Dark Object Subtraction (DOS) approach (Chavez, 1989, 1996), and then converted to surface reflectances. Second, the ETM+ images were classified to produce a land cover map. Using an IKONOS image and 1-m resolution black and white digital orthophotos from the Massachusetts Geographic Information System (Massgis, http://www.state.ma.us/mgis/masgis.htm), the 15 × 13 km Harvard Forest image was classified into broadleaf forests, needleleaf forests, grasses, shrubs, bare land and water using a supervised classification procedure (Fig. 3(b)). With help of an

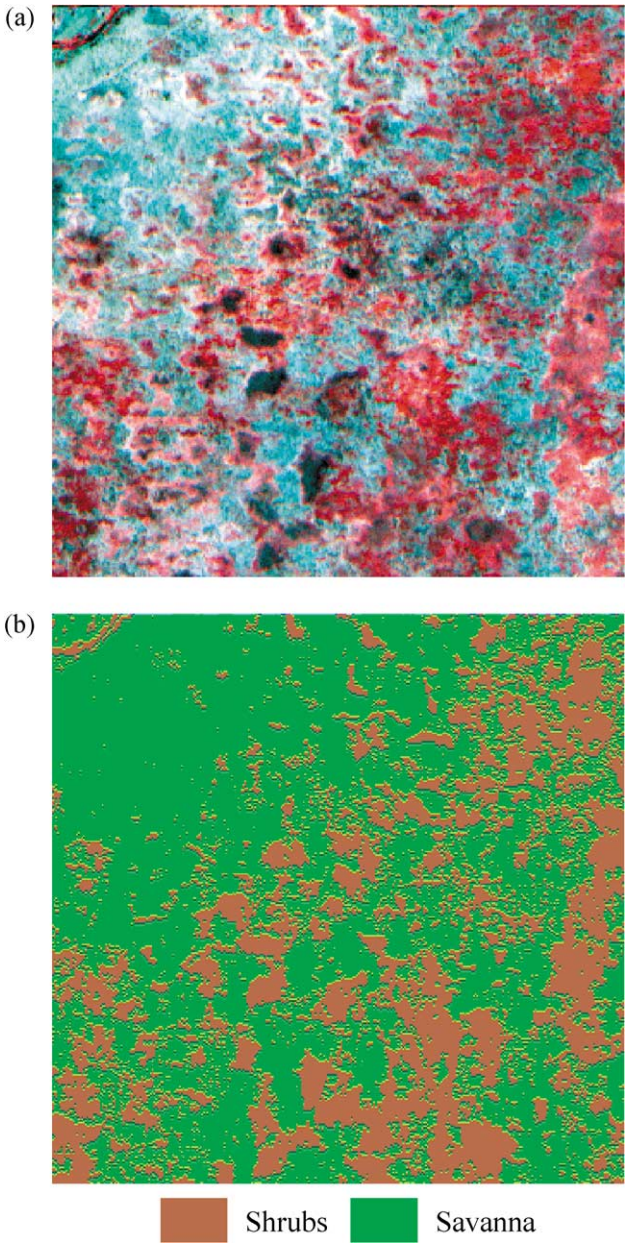

Fig. 2. (a) Color RGB image from Bands 4, 3 and 2 of a 10 × 10 km region of the Maun site from an ETM+ image. (b) Vegetation classification map for the 10 × 10 km region.

IKONOS image and a charge-coupled devices (CCD) image from an aircraft, the 10 × 10 km Ruokolahti Forest image was classified into young, regular and dense needleleaf forests, grasses and water (Fig. 4(b)). The three different needleleaf forests were then merged into one biome type, needleleaf forests. Third, an automated image segmentation procedure (Woodcock & Harward, 1992) was used to produce a region (homogeneous neighborhood) map of each image. For the Harvard Forest site, the minimum region size of 8 ETM+ pixels was used to define regions. Following the definition of regions in the region map, the classification map was overlaid on the region map and each region was

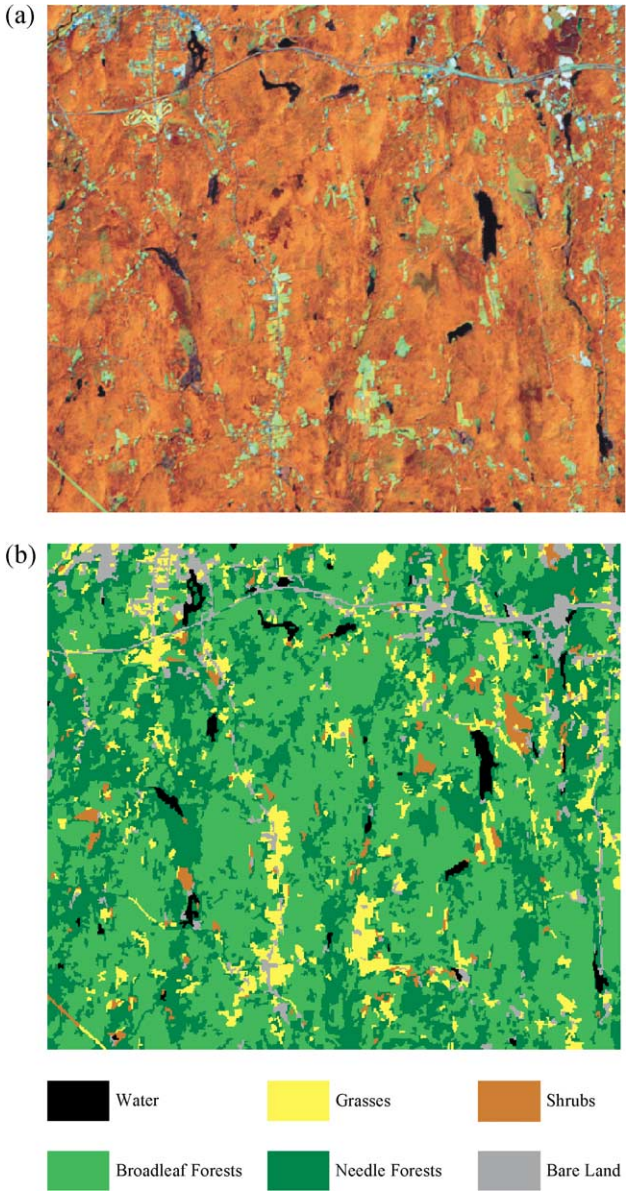

Fig. 3. (a) RGB image of a 15 × 13 km region of Harvard Forest produced from ETM+ Bands 4, 5 and 3. (b) Land cover classification map using supervised classification procedure.

assigned a class label. For the Ruokolahti Forest site, the regions mainly represented the three different forest classes. Finally, we ran the MODIS algorithm to produce LAI for the ETM+ images at 30 m resolution (Fig. 5).

4. Multiscale variation in LAI and NDVI data

We decomposed the LAI data retrieved from ETM+ reflectances at 30-m resolution into a nested hierarchy of classes, regions and pixels, to generate a set of data layers corresponding to the three hierarchical levels for each site using Eqs. (3)–(6). The semivariograms were calculated according to Eq. (9) for each of the decomposed components. NDVI was also included in this analysis in view of its widespread use in vegetation remote sensing.

4.1. Maun

Table 1 lists the distribution of global variance at the class, region and pixel level for the site at Maun following the approaches of Moellering and Tobler (1972) and Collins and Woodcock (2000). Most of the NDVI variance occurs at

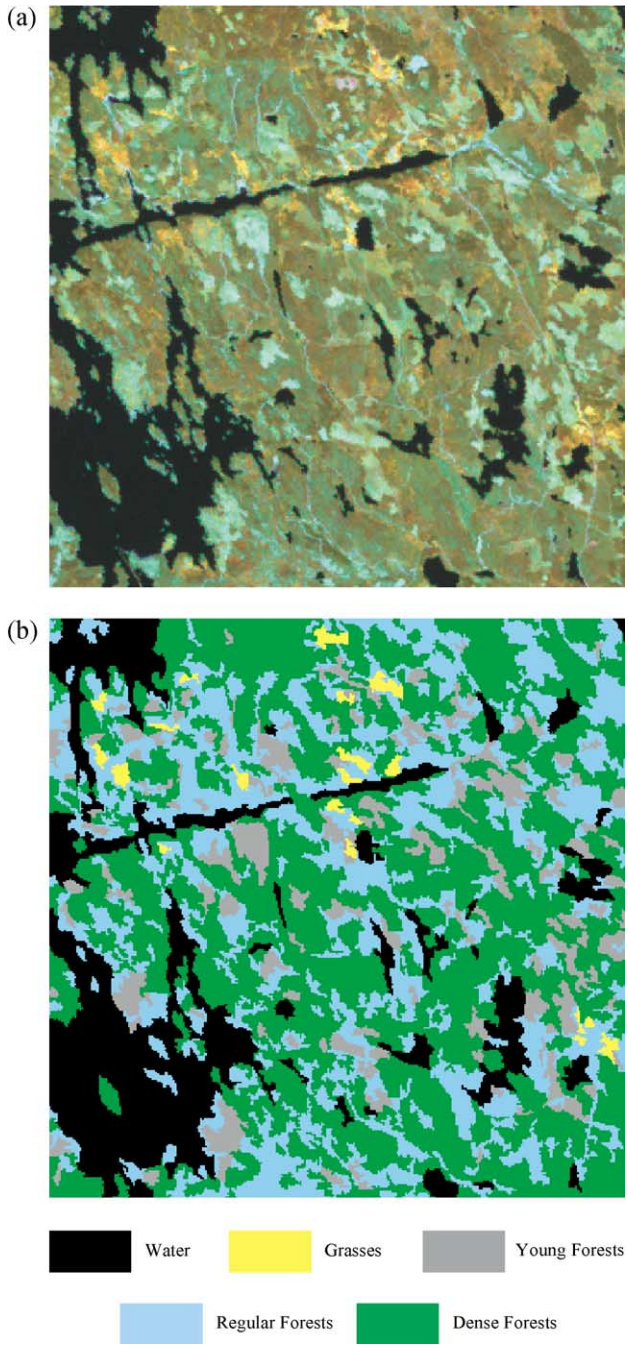

Fig. 4. (a) RGB image of a 10 × 10 km region of Ruokolahti Forest produced from ETM+ Bands 4, 5 and 3. (b) Land cover classification map using supervised classification procedure.

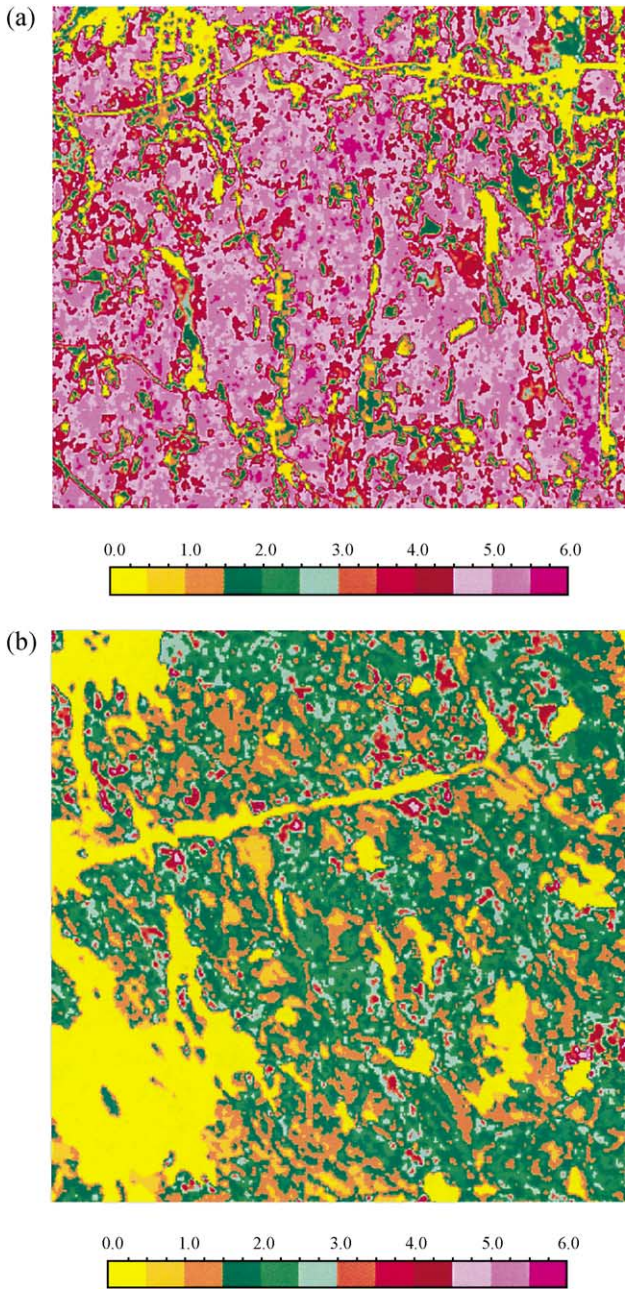

Fig. 5. LAI images from (a) the Harvard Forest site and (b) the Ruokolahti Forest site.

the class (47%) and pixel scales (35%). For the LAI data, the majority of variation is at the pixel (55%), and class scales (32%). Therefore, most of the observed spatial variation of LAI at the Maun site is due to the effect of classes and pixels rather than regions, implying, for example, that shrubs and savanna behave differently from each other (class effect) and there is considerable internal variability within those two classes, but that variability exists at the pixel rather than the patch scale.

While Hierarchical ANOVA quantifies the scale decomposition of variance, examining the semivariograms can aid understanding of the spatial structure (Collins & Woodcock, 2000). Fig. 6(a) and (b) shows the semivariograms of the NDVI and LAI data. Sill heights are close approximations of data variance, so these figures provide a graphic illus-

Table 1
Hierarchical model results for the Maun scenes

Scene	Image	Variance	Percentage of variance (%)
NDVI	original image	0.006956	100
	class effect	0.003263	46.52
	region effect	0.001257	18.07
	pixel effect	0.002436	35.02
LAI	original image	0.18936	100
	class effect	0.06044	31.92
	region effect	0.02502	13.21
	pixel effect	0.10391	54.87

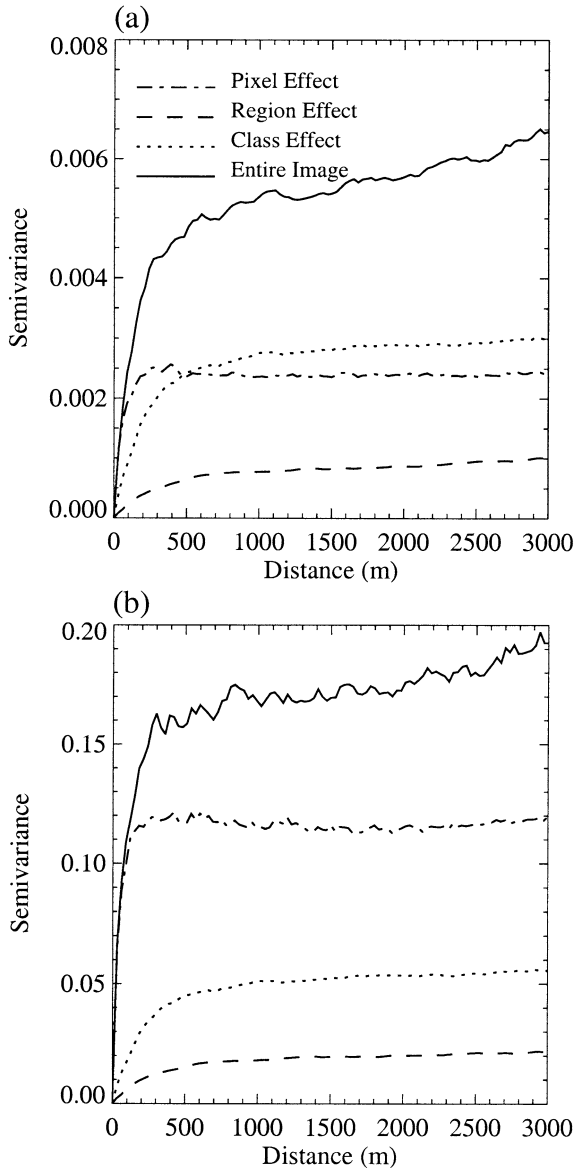

Fig. 6. Hierarchical decomposion of semivariograms for (a) NDVI and (b) LAI of the Maun site.

Table 2
Hierarchical model results for the Harvard forest scenes

Scene	Image	Variance	Percentage of variance (%)
NDVI	original image	0.008365	100
	class effect	0.004991	59.66
	region effect	0.002189	26.17
	pixel effect	0.001185	14.17
LAI	original image	2.7476	100
	class effect	2.1032	76.55
	region effect	0.3147	11.45
	pixel effect	0.3296	11.99

tration of the information contained in Table 1. The semivariance of the original image, $\gamma(h)$, exhibits the highest sill, as it contains the effects of all scales. It initially increases quickly as a function of lag and later gradually throughout the remainder of the graph.

The semivariograms of the class, region and pixel scales are different. For both the NDVI and LAI data, the pixel scale semivariogram reaches a sill at about 200 m (range), and remains flat at larger lags. The class scale semivariogram reaches the sill at about 500 m, and still increases slowly, which indicates that there are objects larger in size than the 3000-m range. This interpretation is supported by Fig. 6 in Tian et al. (2002), which shows that the savanna exceeds this size in the upper left corner. The range is related to the size of objects in the image. Therefore, these plots give an indication of the spatial structure of the effects, in addition to partitioning of the variance.

There is a stronger pixel effect on the LAI than NDVI, which indicates that there is less difference between vegetation classes in the mean value of LAI than NDVI. The large variance and small range (200 m) at the pixel scale are consistent with field measurements (Tian et al., 2002), which indicates that most LAI changes in Maun occur at distances smaller than vegetation stands. The reason for the different effect of classes on NDVI and LAI is that for the same input reflectance, that is, the same NDVI, savanna results in a higher LAI value than shrub. However, shrubs have higher NDVI values than savanna in the ETM+ images. Thus, smaller differences in mean LAI values of savanna and shrubs result from the MODIS LAI algorithm.

These results indicate that the dominant factor influencing the spatial distribution of LAI across the landscape in Maun is variability within land cover types as opposed to differences between land cover types. The strong spatial heterogeneity observed in the field LAI measurements indicates that for validation at the pixel level, individual field measurements must have GPS readings accurate to within a few meters, and the accuracy of geo-registration of ETM+ images should be within half a pixel.

The variance of LAI retrieved from ETM+ data is much smaller than the field measurements taken by LAI-2000 plant canopy analyzer (Fig. 4 in Tian et al., 2001 and Fig. 6), which indicates that the resolution of the LAI-2000 is finer than 30 m. Several measurements in one 30-m resolution pixel are needed for a pixel-by-pixel comparison. These requirements, that is, accurate GPS readings and geo-registration and a large number of measurements within each pixel, make pixel-by-pixel validation risky if the spatial accuracies of GPS and image registration are not achieved. A region-by-region (or patch-by-patch) comparison is a more conservative alternative.

4.2. Harvard forest

The decomposition of variance for the Harvard Forest site is listed in Table 2, and the semivariograms of the three-level hierarchy are shown in Fig. 7. The majority of variation, 59.66% in the NDVI data and 76.55% in the LAI data, is at the scale of classes. Both the region and pixel

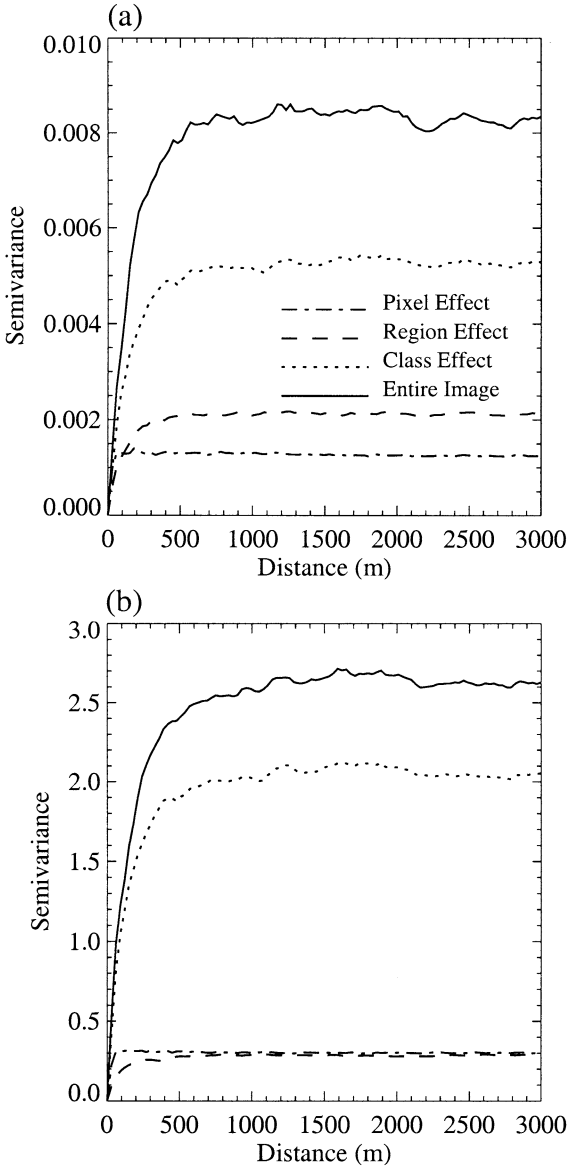

Fig. 7. Hierarchical decomposition of semivariograms for (a) NDVI and (b) LAI of the Harvard Forest site.

variation are relatively small. For both the NDVI and LAI data, the pixel semivariograms reach their sill at about 60 m and remain flat for all larger lags. The range for the semivariogram of class scale is about 500 m, which is roughly twice that of the region scale.

The class effect contributes more variance (76.55%) in the LAI data than the NDVI data (59.66%). The variance of the region effect decreases to 11% in the LAI data, compared with 26.17% in the NDVI data. The relatively higher variance of the class effect indicates that there are large differences between the means of different land cover types. For example, broadleaf forests have mean LAI values as large as 5, compared to zero LAI values for water or bare land. Thus, the LAI values at this site depend strongly on the land cover types to which the pixels belong. Within a vegetation type, the LAI variation among pixels contributes only about 23.45% of total variance. Hence, the LAI at the Harvard Forest site is relatively homogeneous within classes, but varies strongly among classes.

4.3. Ruokolahti forest

At the Ruokolahti site, the class effect contributes the most (93.56%) to the total NDVI variance (Table 3). Of the total LAI variance, the class, region and pixel effects explain 47.78%, 14.41% and 37.7%, respectively. The semivariogram of pixel scale reaches its sill at roughly 300 m, while the range for the region scale semivariogram is about 400–500 m (Fig. 8). The semivariogram of class scale reaches the sill at about 1000 m, and still increases slowly. The NDVI spatial variation is almost completely determined by the class effect. The LAI spatial structure, however, is determined not only by the class effect, but also by the pixel effect, as at Maun.

The very small region scale variation in both NDVI and LAI data is unexpected, because individual patches associated with harvesting and subsequent plantations can be easily distinguished in a RGB ETM+ image of bands 4, 5 and 3. In the NDVI image (Fig. 9), however, these features are blurred, possibly for two reasons. First, histograms of NDVI from young, regular and dense forests (Fig. 10) indicate that the NDVI of regular and dense needleleaf forests are very similar. This is because smaller values of both RED and NIR reflectance of the dense forests result in indistinct NDVI values. Second, although variations in the NDVI data among regions are small, they are large within regions, especially in the case of young and regular forests, which is also seen in the CCD aircraft photographs. This possibly explains the dominance of the pixel effect.

Table 3
Hierarchical model results for the Ruokolahti forest scenes

Scene	Image	Variance	Percentage of variance (%)
NDVI	original image	0.068958	100
	class effect	0.006452	93.56
	region effect	0.001422	2.62
	pixel effect	0.003016	4.37
LAI	original image	1.11046	100
	class effect	0.53058	47.78
	region effect	0.16002	14.41
	pixel effect	0.41985	37.7

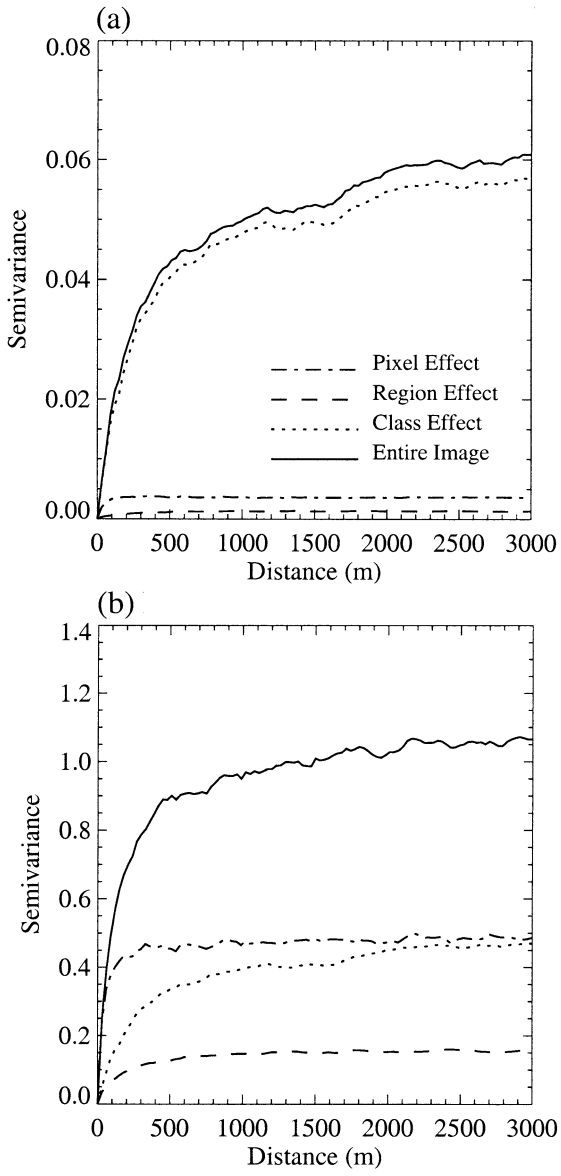

Fig. 8. Hierarchical decomposition of semivariograms for (a) NDVI and (b) LAI of the Ruokolahti Forest site.

The algorithm retrievals compare well with the field measurements in the case of dense and regular forests, but not in young forests. This could be a reason that the region effect does not contribute much to the spatial variation in the LAI data. Improvements to the algorithm are therefore necessary.

4.4. Comparison of scale effects between sites

There are very different patterns of LAI variance with respect to the three levels of landscape organization. At

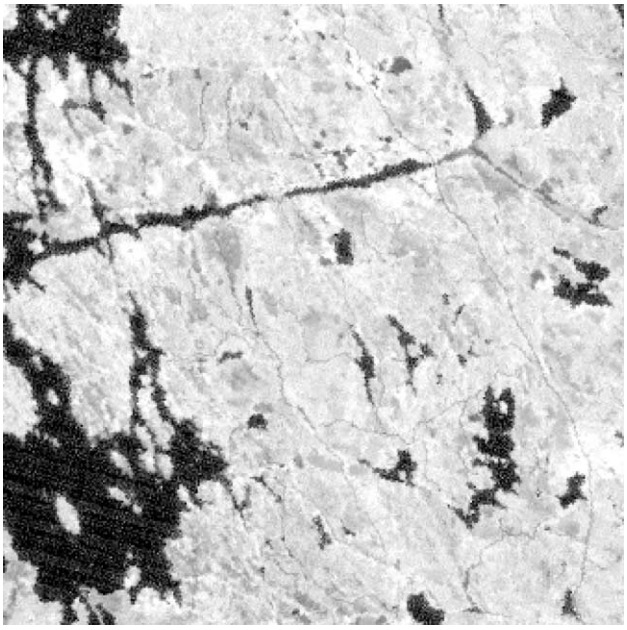

Fig. 9. The NDVI image from the Ruokolahti Forest site. The color from black to white represents the range of NDVI values. The brighter the image, the larger the NDVI value.

Maun, the pixel effect is dominant, while at the Harvard Forest site the class effect contributes most to the variance. At the Ruokulahti Forest site, both the class and pixel effect are equally important in determining the spatial variation of LAI. A question of some importance is, under what circumstances is the spatial distribution of LAI across the landscape due to variations within land cover types as opposed to differences between land cover types? The coefficients of variation (standard deviation/mean, COV) of NDVI and LAI at the three sites are listed in Table 4. The NDVI data from Maun and Ruokolahti show a similarity: the COV within classes is relatively larger than that from the Harvard Forest, especially for the dominant class type (savanna in Maun, broadleaf forests in the Harvard Forest, and needleleaf forests in the Ruokolahti Forest). Although most spatial variation occurs at the class scale in the NDVI data, the large COV within classes results in a large spatial variation within classes in the LAI retrievals. As a result, the majority of spatial variation is first at the scale of pixel in the LAI data. On the other hand, the Harvard Forest exhibits smaller COV in NDVI, thus, less spatial variation at the pixel scale in the LAI data. Thus, whether the spatial distribution of LAI across the landscape is due to variations within land cover types depends on the homogeneity within the land cover, especially the dominant class type. The validation of homogeneous broadleaf forests will be relative easier than savanna or needleleaf forests. The latter require more accurate GPS readings and scientific sampling strategy to capture the spatial variation of LAI.

The range of semivariograms is indicative of the size of the largest elements (objects) in the scale. The <500-m range in the semivariograms of class scale at Maun and Harvard Forest sites indicates that landscape variations occur over relative small areas. Land cover generally varies beyond 500 m. This also indicates that the 1-km MODIS pixels are generally mixed pixels. Ranges in semivariograms of pixel scale from the three sites suggest that no variation at scales finer than regions could be detected at resolutions coarser than 200 m. Therefore, validation needs to be performed in small regions (<500 m).

Results from Tables 1–3 indicate that the region effect always contributes 10–15% of spatial variation in the LAI data. This is why one could and should use the segmentation procedure to compare field data with fine resolution satellite

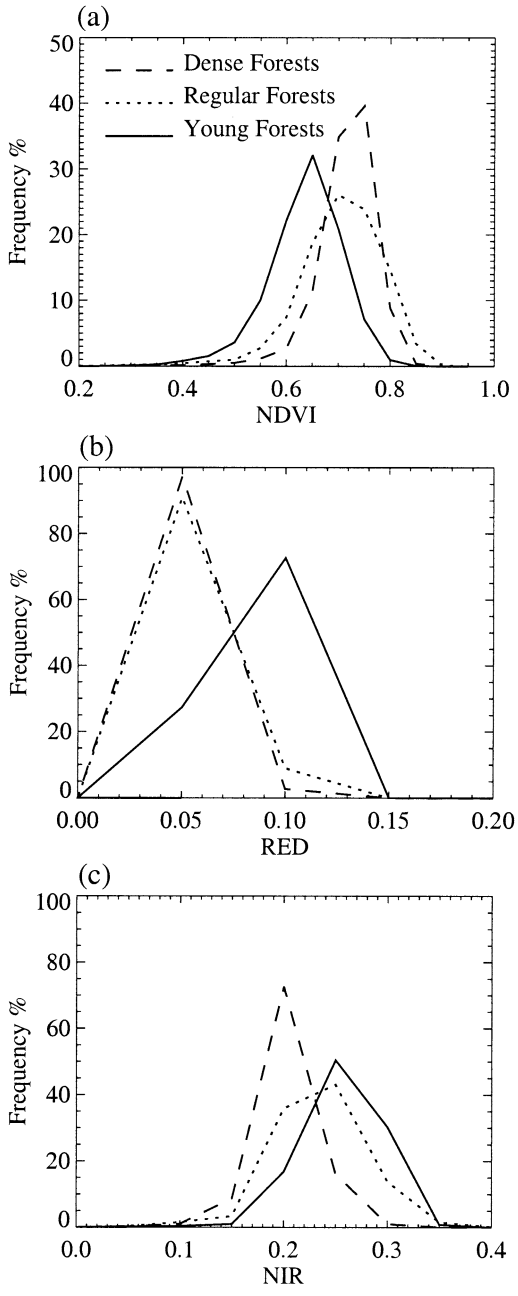

Fig. 10. Histograms of (a) NDVI, (b) RED and (c) NIR for young, regular and dense forests at the Ruokolahti Forest site.

Table 4
Coefficients of variation of NDVI and LAI from different biome types and sites

Site Name	Biome Type	NDVI	LAI
Maun	shrubs	0.0953	0.3596
	savanna	0.1314	0.4622
Farvard Forest	grasses	0.1104	0.2438
	shrubs	0.0601	0.1474
	broadleaf forests	0.0260	0.1423
	needleleaf forests	0.0561	0.2756
Ruokolahti Forest	grasses	0.1502	0.2566
	total needleleaf forests	0.1066	0.4306
	young needleleaf forests	0.1187	0.4357
	regular needleleaf forests	0.1230	0.5271
	dense needleleaf forests	0.0806	0.3181

retrievals (Tian et al., 2002), especially at sites (e.g., the Harvard Forest and Ruokulahti Forest sites) where the pixel scale variation is small.

The decomposition of semivariograms according to the hierarchical model shows the relative contribution of different characteristic scales to the overall variation. This method also displays the spatial structure of the different scales within a scene. Knowledge gained from these analyses can influence data collection practices. For a homogeneous (within class) site such as broadleaf forests of the Harvard Forest, where the class and region effect account for 90% of the spatial variation, a sampling strategy should focus more on using accurate land cover maps and selection of regions. However, for a heterogeneous (within class) site such as needleleaf forests of the Ruokulahti Forest or savanna of Maun, accurate point measurements within GPS readings are needed. The fine resolution of LAI-2000 makes it difficult to quantify the relation between field measurements and satellite retrievals. Therefore, either the number of point measurements within 30-m resolution should be increased, or a region-by-region comparison should be attempted.

The absolute magnitudes of variance vary significantly across the three sites. The overall variance in the LAI data is only 0.2 in Maun, compared to 2.5 at Harvard Forest; even the pixel effect variance here is larger than the total variance in Maun. Higher variance is equivalent to higher information content. The Harvard Forest site contains more spatial information than Maun.

In this study, we find that the spatial structure of NDVI is not similar to that of LAI, due to the nonlinear relation between NDVI and LAI. It may also be due to certain limitations of the LAI/FPAR algorithm. It should be noted that the algorithm does not use NDVI–LAI relations for LAI retrievals.

Based on our study, here we propose the following sampling and validation strategy:

1. Classifying an ETM+ image of the validation site over a roughly 10 × 10 km area, and identifying the major class types.
2. Segmenting the classified map into the region (patch) level map.
3. Partitioning the LAI image estimated from the algorithm into the class, region and pixel scale; calculating semivariograms of the decomposed components; identifying the contribution of variation from each effect; and evaluating the range of these semivariograms and obtaining a general idea of the size of objects in the images.
4. Determining where to collect field measurements and how to sample measurement points over the 10 by 10 km area based on the analysis from step 3, making certain that the major class types have a dozen or more regions of field measurements; the minor class types should also have several regions in order to stratify the whole area.
5. Taking ground measurements of LAI.
6. Validating the MODIS LAI algorithm with the ETM+ image first, either based on the region level or pixel level, and producing a 10 × 10 km LAI map using the validated algorithm.
7. Comparing the MODIS 1 km LAI products to the ETM+ retrievals.

5. Concluding remarks

Validation of global satellite data products is crucial, both to establish the accuracy of the products for the science-user community and to provide feedback to improve the data processing algorithms (Cohen & Justice, 1999). The development of appropriate ground-based validation techniques is therefore important to assess the uncertainties associated with such data products. In this two-part series, we attempted to assess the uncertainty of the MODIS LAI product via comparisons with ground and high-resolution satellite data, and developed guidance for field data collection and sampling strategies.

This paper (Part II) attempted to define sampling strategies based on hierarchical analysis of LAI fields retrieved from 30-m resolution ETM+ data by the MODIS algorithm. With a hierarchical scene model, we divided LAI and NDVI images from Maun (Botswana), Harvard Forest (USA) and Ruokulahti Forest (Finland) into individual scale images of class, region and pixel. Isolating the effects associated with different landscape scales through decomposition of semivariograms not only showed the relative contribution of different characteristic scales to the overall variation, but also displayed the spatial structure of the different scales within a scene. We found that (1) patterns of variance at the class, region and pixel scale at these sites are different with respect to the dominance in order of the three levels of landscape organization within a scene; (2) the spatial structure of LAI showed similarity across the three sites, that is, ranges of semivariograms from scale of pixel, region and class are less than 1000 m. (3) validation needs to be performed over smaller regions or patches, with more field

measurements and at smaller intervals; (4) the spatial structure of the NDVI is not the same as that of LAI; and (5) the absolute magnitudes of variance vary significantly across the three sites.

Knowledge gained from these analyses aids us in formulation of sampling strategies for validation of biophysical products derived from moderate resolution sensors. For a homogeneous (within class) site, where the scales of class and region account for most of the spatial variation, a sampling strategy should focus more on using accurate land cover maps and selection of regions. However, for a heterogeneous (within class) site, accurate point measurements and GPS readings are needed. For field validation of LAI, due to the fine resolution of LAI-2000 measurement and georegistration accuracy, it is difficult to quantify the relation between field measurements and 30-m resolution satellite retrievals. One should either increase the number of point measurements within 30-m resolution, or use a region-by-region comparison for validation of heterogeneous sites. These constraints imply that for validation activity, selecting the sample scale on the basis of the underlying spatial structure of the landscape (as understood through hierarchical decomposition of semivariograms) is necessary and in general, patches are better than individual pixels unless sample and registration accuracy are outstanding.

Acknowledgements

We thank the three anonymous reviewers for their professional and insightful comments. We also thank individuals who participated in the SAFARI 2000 wet season, Harvard Forest, and Ruokolahti Forest campaigns, especially Luanne Otter, Robert Scholes, Seth Hoffman, and Pauline Stenberg; the people who were essential in acquiring and processing the ETM+ and IKONOS data, especially Jeff Morisette, Heikki Smolander; and all the various other field participants who made various measurements that we used, especially Grace Smith, and Karyn Tabor. This study was part of the SAFARI 2000 Southern African Regional Science Initiative. The research work was supported by NASA through MODIS Contract NAS5-96061.

References

Chavez, P. S. (1989). Radiometric calibration of Landsat Thematic Mapper multispectral images. *Photogrammetric Engineering & Remote Sensing*, *55*, 1285–1294.

Chavez, P. S. (1996). Image-based atmospheric corrections-Revisited and improved. *Photogrammetric Engineering & Remote Sensing*, *62*, 1025–1036.

Cohen, W. B., & Justice, C. O. (1999). Validating MODIS terrestrial ecology products: linking in situ and satellite measurements. *Remote Sensing of Environment*, *70*, 1–3.

Collins, J. B., & Woodcock, C. E. (2000). Combining geostatistical methods and hierarchical scene models for analysis of multiscale variation in spatial data. *Geographical Analysis*, *32*(1), 50–63.

Curran, P. J. (1988). The semivariogram in remote sensing: an introduction. *Remote Sensing of Environment*, *37*, 493–507.

Justice, C., Belward, A., Morisette, J., Lewis, P., Privette, J., & Baret, F. (2000). Developments in the 'validation' of satellite sensor products for the study of the land surface. *International Journal of Remote Sensing*, *21*(17), 3383–3390.

Knyazikhin, Y., Glassy, J., Privette, J.L., Tian, Y., Lotsch, A., Zhang, Y., Wang, Y., Morisette, J.T., Votava, P., Myneni, R.B., Nemani, R.R., & Running S.W. (1999). MODIS Leaf Area Index (LAI) and Fraction of Photosynthetically Active Radiation Absorbed by Vegetation (FPAR) Product (MOD15) Algorithm. Theoretical Basis Document, NASA Goddard Space Flight Center, Greenbelt, MD 20771, USA.

Knyazikhin, Y., Martonchik, J. V., Diner, D. J., Myneni, R. B., Verstraete, M. M., Pinty, B., & Gobron, N. (1998). Estimation of vegetation canopy leaf area index and fraction of absorbed photosynthetically active radiation from atmosphere-corrected MISR data. *Journal of Geophysical Research*, *103*, 32239–32256.

Knyazikhin, Y., Martonchik, J. V., Myneni, R. B., Diner, D. J., & Running, S. W. (1998). Synergistic algorithm for estimating vegetation canopy leaf area index and fraction of absorbed photosynthetically active radiation from MODIS and MISR data. *Journal of Geophysical Research*, *103*, 32257–32275.

Lucht, W., Hyman, A. H., Strahler, A. H., Barnsley, M. J., Hobson, P., & Muller, J. (2000). A comparison of satellite-derived spectral albedos to ground-based broadband albedo measurements modeled to satellite spatial scale for a semidesert landscape. *Remote Sensing of Environment*, *74*, 85–98.

Moellering, H., & Tobler, W. (1972). Geographical variance. *Geographical Analysis*, *4*, 34–64.

Privette, J. L., Asner, G. P., Conel, J., Huemmrich, K. F., Olson, R., Rango, A., Rahman, A. F., Thome, K., & Walter-Shea, E. A. (2000). The EOS prototype validation exercise (PROVE) at Jornada: overview and lessons learned. *Remote Sensing of Environment*, *74*, 1–12.

Tian, Y., Woodcock, C. E., Wang, Y., Privette, J. L., Shabanov, N. V., Zhou, L., Zhang, Y., Buermann, W., Dong, J., Veikkanen, B., Hame, T., Andersen, K., Ozdogan, M., Knyazikhin, Y., & Myneni, R. B. (2001). Multiscale analysis and validation of MODIS LAI product. Uncertainty assessment. *Remote Sensing of Environment*, *83*, 415–431 (this issue).

Weiss, M., Beaufor, L., Baret, F., Allard, D., Bruguier, N., & Marloie, O. (2001). Leaf area index measurements at different scales for the validation of large swath satellite sensors: first results of the VALERI project. *Proceeding of the 8th international symposium on physical measurements and signatures in remote sensing* (pp. 125–130).

Woodcock, C. E., Collins, J. B., & Jupp, D. L. B. (1997). Scaling remote sensing models. In P. R. Van Gardingen, G. M. Foody, & P. J. Curran (Eds.), *Scaling-up from cell to landscape* (pp. 61–77) (Cambridge, United Kingdom).

Woodcock, C. E., & Harward, V. J. (1992). Nested-hierarchical scene models and image segmentation. *International Journal of Remote Sensing*, *13*(16), 3167–3187.

Woodcock, C. E., Strahler, A. H., & Jupp, D. L. B. (1988a). The use of variograms in remote sensing: I. Scene models and simulated images. *Remote Sensing of Environment*, *25*, 323–348.

Woodcock, C. E., Strahler, A. H., & Jupp, D. L. B. (1988b). The use of variograms in remote sensing: II. Real digital images. *Remote Sensing of Environment*, *25*, 349–379.